On the Impact of Substrate Contact Resistance in Bifacial MIS-type Lifetime Structures

Axel Herguth[1, a)], Fabian Kostrzewa and David Sperber

[1]University of Konstanz, Department of Physics, 78457 Konstanz, Germany

[a)]Corresponding author: axel.herguth@uni-konstanz.de

Abstract. Bifacial metal-insulator-semiconductor (MIS) structures are used to intentionally manipulate field-effect passivation of dielectric layers on crystalline silicon substrates during lifetime measurements by external biasing. It is found that the impact of biasing on surface passivation depends on the quality of the substrate contact, in particular in asymmetric front/rear biasing conditions. A mathematical model is presented demonstrating the problems arising from a high substrate contact resistance.

INTRODUCTION

Field effect passivation is the dominant passivation mechanism for dielectric layers carrying a fixed charge density, be it positive like in SiN_x:H, or negative like in AlO_x:H [1]. It can be shown that the surface recombination described in a J_0 formalism scales with (sufficiently high) fixed charge density Q_f and surface recombination velocity S at the surface: $J_0 \propto S/Q_f^2$ [2].

Even though it is in certain situations possible to separate recombination in the bulk and at the surface by its characteristic injection dependence, it is close to impossible to further separate the impact of S (chemical component of surface passivation) and Q_f (field effect component of surface passivation) in a 'normal' lifetime measurement. This limitation can be overcome if one of these quantities can be deliberately manipulated. Fixed charge density Q_f can, e. g., be reversibly compensated by depositing rather volatile charged air molecules/radicals created by a corona discharge, e. g. [3] [4].

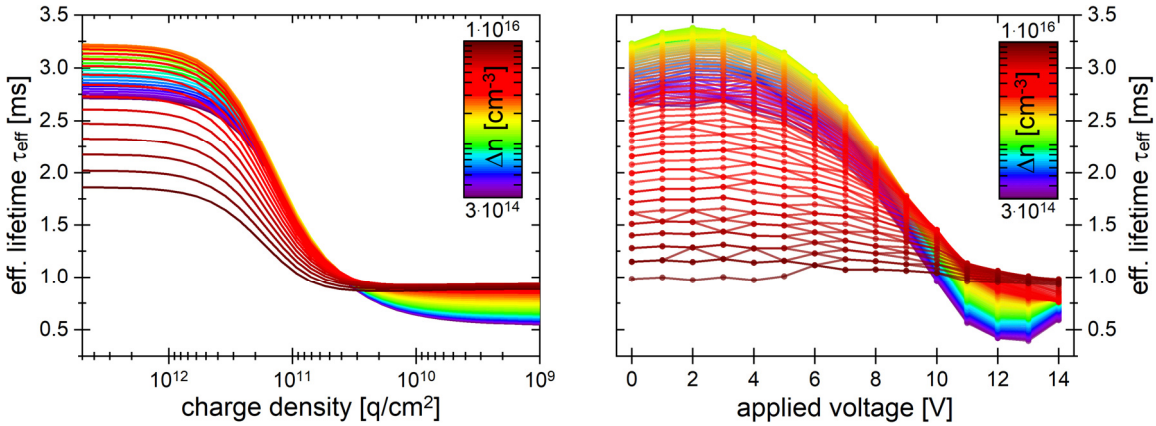

Figure 1. (left) Simulated injection-dependent effective lifetime vs. charge density calculated with PC1D 6.2 [5]. (right) Measured lifetime measurement series with increasing voltage for a monofacial SiN_x:H/AlO_x:H stack.

Another approach is to create a metal-insulator-semiconductor (MIS) structure by depositing an electrode on the dielectric passivation layer of thickness w, thus creating a plate capacitor with areal capacity $C = \varepsilon_0 \varepsilon_{\mathrm{di}}/w$. Applying a voltage V to this plate capacitor means to charge it with a charge density $Q = C \cdot V$, thus (over-) compensating the fixed charge density Q_{f} and suppressing field effect passivation. The impact on effective lifetime is exemplarily depicted in Fig. 1 (left: PC1D simulation [5], right: experimental data for a SiN_x:H/AlO_x:H layer stack). This technique has been successfully applied before using, e. g., ultrathin semi-transparent metallic electrodes [6, 7], semi-transparent polycrystalline silicon electrodes [8], transparent PEDOT:PSS electrodes [9] or opaque single-sided electrodes [10].

EXPERIMENTAL DETAILS AND RESULTS

For a concept study of bifacial MIS-type lifetime structures, FZ-Si samples (1 Ωcm, 250 µm thick, 5 × 5 cm²) were passivated bifacially with ~25 nm AlO_x:H deposited via plasma-assisted atomic layer deposition (PEALD) in a FlexAl tool (Oxford Instruments). Note that ALD yields pinhole-lean but not perfectly pinhole-free dielectric layers. In order to create semi-transparent MIS structures, a thin layer of aluminum (5-10 nm) was deposited via thermal evaporation on front and rear surface covering the central part of the sample that is sensitive to a PCD measurement done by a WCT-120 lifetime tester (Sinton Instruments) [11]. By masking during evaporation, a separated substrate contact area was created in which the AlO_x:H layer was removed by scratching before evaporation. In addition, proper masking prevents undesired contact between front and rear Al layer. Hence, a sample features three independent electrodes: the metallic Al electrodes of the MIS structures on the front and rear side as well as a substrate electrode.

By applying a voltage to the MIS electrode with respect to the grounded substrate contact, the field effect passivation of the MIS structure was manipulated during PCD measurements to neutralize step-by-step the influence of the fixed charges in the AlO_x:H layers, and to reveal the chemical passivation component. As it was suspected that fixed charge densities of front and rear side might differ, and that a different voltage could be needed to compensate the respective fixed charge densities, individual voltages V_{F} and V_{R} were applied to front and rear MIS electrodes.

Measurements across the MIS structures indicated leakage currents (probably via pinholes) in the µA-range, or in other words, MIS shunt resistances in the 100 kΩ range. It was noted as well that contacting the substrate properly failed and resulted in an unintentionally high substrate contact resistance of ~50 kΩ. This is probably due to a bad combination of a rough (scratched) surface covered by an Al layer too thin to compensate for this roughness plus maybe made even worse by native oxide. Later sample generations did not show this issue any more. Even though these samples are certainly far from ideal, analyzing the results is nevertheless quite instructive and nicely shows the impact (and danger) of substrate contact resistance in a MIS-type lifetime structure.

Figure 2 shows the effective lifetime results of a PCD measurement series, on the left side plotted versus injection Δn at various front side voltages V_{F}, on the right side versus applied front voltage V_{F} at various injection levels Δn. Rear side voltage was adapted as well as can be seen from the ratio graph on the right side of Fig. 2. As can be seen, effective lifetime keeps dropping with increasing front and rear side voltage – just as expected. However, the measurement at V_{F} = 4.8 V breaks ranks. Strikingly, it is precisely the measurement where rear voltage V_{R} was not kept at a constant ratio to V_{F}. A look at the mathematics in the background helps to understand this behavior.

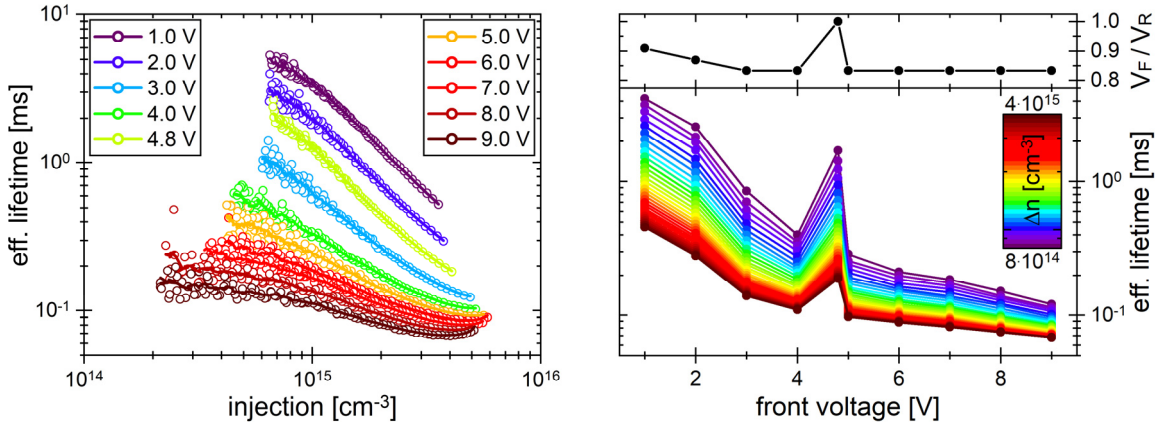

Figure 2. (left) Injection-dependent effective lifetime data measured by PCD at different applied front voltages V_{F}. (right) Effective lifetime plotted versus applied front voltage. Rear voltage V_{R} can be deduced from $V_{\mathrm{F}}/V_{\mathrm{R}}$ ratio.

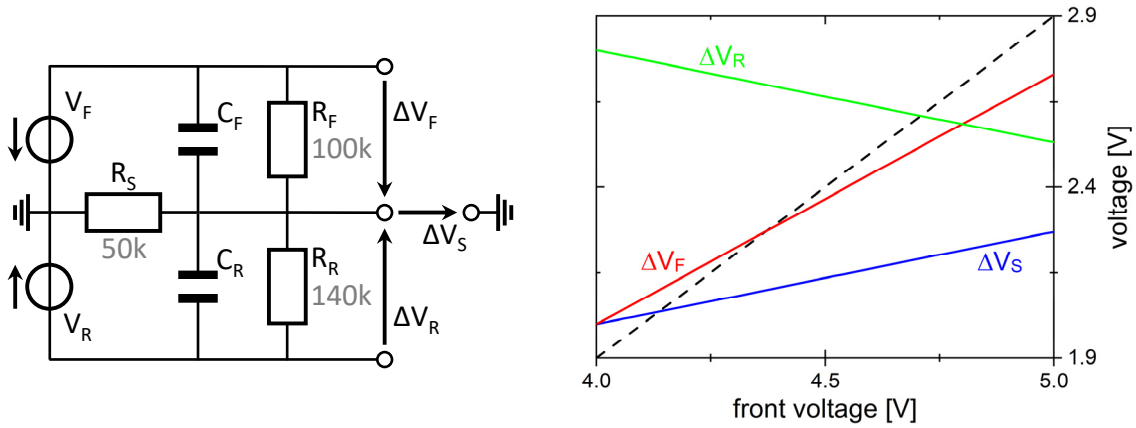

Figure 3. (left) Equivalent circuit diagram including values for the different resistive elements consistent with the observations from Fig. 2. (right) Change in voltage drops across the resistive elements during the side step of V_F from 4.0 V to 4.8 V in Fig. 2 while keeping V_R = 4.8 V constant.

MATHEMATICAL MODEL

An equivalent circuit diagram is given on the left hand side of Fig. 3. The MIS structures on the front and rear side act as capacitive elements C_F and C_R supplied by the voltages V_F and V_R (relative to ground). In parallel, the shunt resistances R_F and R_R allow for leakage currents I_F and I_R. The substrate is contacted via the resistor R_S to ground. Ohm's law yields the equation system

$$\Delta V_F = V_F - \Delta V_S = R_F \cdot I_F \tag{1}$$

$$\Delta V_R = V_R - \Delta V_S = R_R \cdot I_R \tag{2}$$

$$\Delta V_S = R_S \cdot I_S = R_S \cdot (I_F + I_R) \tag{3}$$

with ΔV_F, ΔV_R, ΔV_S being the voltage drops across the resistances R_F, R_R, R_S. Note that ΔV_F and ΔV_R are the voltages relevant for field effect passivation on the front and rear. Solving for those voltage drops yields the general solution

$$\Delta V_S = \left(1 + \frac{R_S}{R_F} + \frac{R_S}{R_R}\right)^{-1} \cdot \left[\frac{R_S}{R_F} \cdot V_F + \frac{R_S}{R_R} \cdot V_R\right] \tag{4}$$

$$\Delta V_F = \left(1 + \frac{R_S}{R_F} + \frac{R_S}{R_R}\right)^{-1} \cdot \left[V_F + \frac{R_S}{R_R} \cdot (V_F - V_R)\right] \tag{5}$$

$$\Delta V_R = \left(1 + \frac{R_S}{R_F} + \frac{R_S}{R_R}\right)^{-1} \cdot \left[V_R - \frac{R_S}{R_F} \cdot (V_F - V_R)\right] \tag{6}$$

with V_F and V_R as experimentally accessible parameters as well as R_F, R_R and R_S as sample specific parameters. Note that the pre-factor is always positive and smaller or equal to unity. The leakage currents I_F and I_R can be easily derived from (1), (2) and (4). Some special cases shall be discussed.

The ideal scenario

In an ideal scenario substrate contact resistance R_S is negligible, thus $R_S \ll R_F$ and $R_S \ll R_R$. Hence, there occurs hardly any voltage drop across R_S, thus $\Delta V_S \to 0$. In consequence, applied voltages fully drop across the MIS structures, thus $\Delta V_F \to V_F$ and $\Delta V_R \to V_R$. Both sides can be manipulated independently of each other applying different voltages V_F and V_R.

The symmetric non-ideal scenario

Unlike the ideal scenario, substrate contact resistance R_S is not negligible, thus $R_S \sim R_F, R_R$. If front and rear side are not biased independently, thus $V_F = V_R = V_{FR}$, there is a finite voltage drop across the substrate resistance

$$\Delta V_S = \left(1 + \frac{R_S}{R_F} + \frac{R_S}{R_R}\right)^{-1} \cdot \left[\frac{R_S}{R_F} + \frac{R_S}{R_R}\right] \cdot V_{FR} \tag{7}$$

which depends on the ratio of R_S and MIS structure shunt resistances R_F and R_R. As per definition (1,2), voltage drops ΔV_F and ΔV_R across those shunt resistances are the same for $V_F = V_R = V_{FR}$.

$$\Delta V_F = \Delta V_R = \left(1 + \frac{R_S}{R_F} + \frac{R_S}{R_R}\right)^{-1} \cdot V_{FR} \tag{8}$$

An increase in applied voltage V_{FR} results in an increase of both, ΔV_F and ΔV_R, however, due to the voltage drop ΔV_S only a fraction of the applied voltage V_{FR} lies across the MIS structure. The disadvantage of the symmetrically applied voltage is that it does not allow for an individual adjustment of field effect passivation for the front and rear side MIS structure in case of different fixed charge densities. Assuming, e. g., the resistance given in Fig. 3, only half (~54 %) of the symmetrically applied voltage V_{FR} would drop at the MIS structures.

The asymmetric non-ideal scenario

The individual, asymmetric adjustment of applied front and rear voltages V_F and V_R results in the non-ideal scenario in peculiar side effects. Assuming a relationship $V_R = V_{R0} + x_i \cdot V_F$, thus $x = dV_R/dV_F$, the voltage drops ΔV_F (5) and ΔV_R (6) read as

$$\Delta V_F = \left(1 + \frac{R_S}{R_F} + \frac{R_S}{R_R}\right)^{-1} \cdot \left\{\left[1 + \frac{R_S}{R_R} \cdot (1 - x)\right] \cdot V_F - \frac{R_S}{R_R} \cdot V_{R0}\right\} \tag{9}$$

$$\Delta V_R = \left(1 + \frac{R_S}{R_F} + \frac{R_S}{R_R}\right)^{-1} \cdot \left\{\left[x - \frac{R_S}{R_F} \cdot (1 - x)\right] \cdot V_F + \left(1 + \frac{R_S}{R_F}\right) \cdot V_{R0}\right\} \tag{10}$$

As a first side effect, ΔV_F or ΔV_R can turn negative in certain situations even though $V_F > 0$ and/or $V_R > 0$. For example, for $x = 0$ and $V_{R0} = 0$, thus front side operation only with the rear side grounded, ΔV_R turns negative with applied positive V_F even though the rear side is grounded.

A second side effect occurs when changing the applied front side voltage V_F. In certain situations, the derivative of ΔV_F or ΔV_R with respect to V_F changes turns negative.

$$\frac{d}{dV_F}\Delta V_F \leq 0 \quad \text{for} \quad x_1 = \frac{dV_R}{dV_F} \geq 1 + \left[\frac{R_S}{R_R}\right]^{-1} \tag{11}$$

$$\frac{d}{dV_F}\Delta V_R \leq 0 \quad \text{for} \quad x_2 = \frac{dV_R}{dV_F} \leq \left(1 + \left[\frac{R_S}{R_F}\right]^{-1}\right)^{-1} \tag{12}$$

Hence, only for $x_1 > dV_R/dV_F > x_2$ an increase in V_F results in an increase of both, ΔV_F and ΔV_R. Assuming, e. g., the resistance given in Fig. 3, change in ΔV_F and ΔV_R has the same direction only for $0.33 \leq dV_R/dV_F \leq 3.8$. Outside this range, either ΔV_F or ΔV_R decreases even though V_F increases. This scenario is depicted in the contour plots of Fig. 4. The equipotential lines of ΔV_F or ΔV_R correspond to the dV_R/dV_F-slopes of (11) and (12) forming a cone where an increase in V_F yields an increase of both, ΔV_F and ΔV_R. The linked data points represent the measurement series from Fig. 2. Except for the side step at V_R = 4.8 V, the measurement series proceeds within this cone and field effect passivation within the front and rear MIS structure is simultaneously lowered. The side step of V_F from 4.0 V to 4.8 V while keeping V_R = 4.8 V constant occurs with $dV_R/dV_F = 0$ outside of this cone and results in an effective reduction of ΔV_R (Fig. 3 right). Thus field effect passivation within the rear MIS structure improves and causes the observed increase in effective lifetime during the measurement series in Fig. 2.

If a certain combination of ΔV_F and ΔV_R is desired, the necessary combination of V_F and V_R corresponds to the intersection of the ΔV_F- and ΔV_R-equipotential lines in Fig. 4.

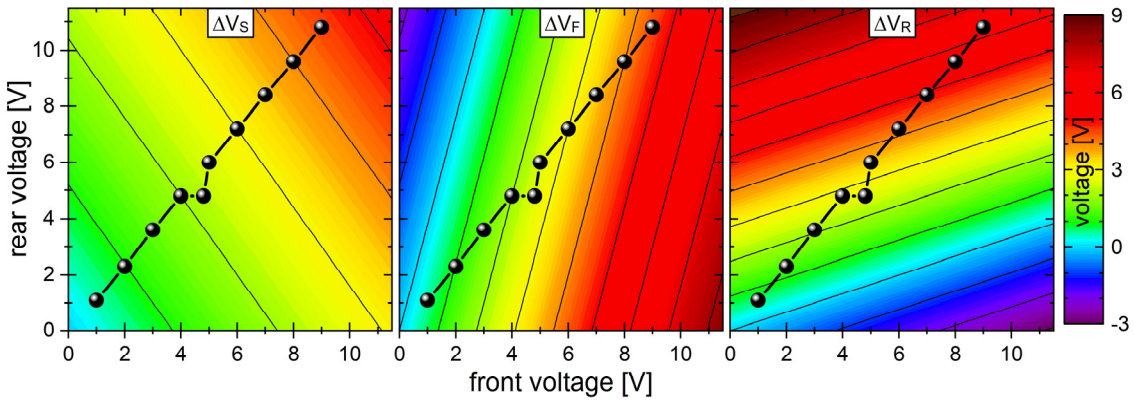

Figure 4. Contour diagrams of the voltage drops across the resistive elements shown in the equivalent circuit diagram in Fig. 3 in dependence of front and rear voltage. Thin black lines correspond to equipotential lines. The linked black data depicts the measurement series from Fig. 2.

CONCLUSIONS

On the one hand, Fig. 1 and (in parts) Fig. 2 demonstrate that MIS-type lifetime structures allow for an advanced lifetime characterization with no more than a turn of the voltage regulator. On the other hand, Fig. 2 illustrates as well how critical the substrate contact resistance is for proper analysis of MIS-type lifetime structures. It is important to note that applied voltage does not necessarily drop at the MIS structure regardless of whether it is a mono- or bifacial configuration. In the bifacial configuration, the situation can become even more difficult to assess if front and rear voltage are adjusted individually. The best way to avoid these issues is certainly to ensure a reliable and sufficiently good substrate contact.

REFERENCES

1. R. S. Bonilla, B. Hoex, P. Hamer and P. R. Wilshaw, Phys. Stat. Sol. (a) **214**, 1700293 (2017).
2. K. R. McIntosh and L. E. Black, J. Appl. Phys. **116**, 014503 (2014).
3. R. B. Comizzoli, J. Electrochem. Soc. **134**, 424-429 (1987).
4. R. S. Bonilla and P. R. Wilshaw, J. Appl. Phys. **121**, 135301 (2017).
5. H. Haug and J. Greulich, Energy Procedia **92**, 60-68 (2016).
6. E. Yablonovitch, R. M. Swanson, W. D. Eades and B. R. Weinberger, Appl. Phys. Lett. **48**, 245-247/1021 (1986).
7. W. E. Jellett and K. J. Weber, Appl. Phys. Lett. **90**, 042104 (2007).
8. R. Girisch, R. Mertens and R. D. Keersmaecker, IEEE Trans. Electron Devices **35**, 203-222 (1988).
9. R. S. Bonilla, Solar RRL **2**, 1800172 (2018).
10. H. Haug, S. Olibet, O. Nordseth and E. S. Marstein, J. Appl. Phys. **114**, 174502 (2013).
11. D. Kiliani, G. Micard, B. Steuer, B. Raabe, A. Herguth and G. Hahn, J. Appl. Phys. **110**, 054508 (2011).